Optimisation of glass and carbon fibre-reinforced concrete with external enzymatic self-healing: an experimental and environmental impact study

buildings

MDPI

Article

Optimisation of Glass and Carbon Fibre-Reinforced Concrete with External Enzymatic Self-Healing: An Experimental and Environmental Impact Study

Mohamed Rabie *, Ali Bahadori-Jahromi and Ibrahim G. Shaaban ‡

Department of Civil Engineering and Built Environment, School of Computing and Engineering, University of West London, London W5 5RF, UK; ali.bahadori-jahromi@uwl.ac.uk (A.B.-J.)

* Correspondence: mohamed.rabie@uwl.ac.uk

‡ Ibrahim G. Shaaban passed away during the preparation of manuscript.

Abstract

This study evaluates glass and carbon fibre-reinforced concrete in terms of performance, durability, environmental impact, and a novel enzymatic self-healing method. An experimental program was conducted on seven concrete mixes, including a plain control and mixes with varying dosages of glass and carbon fibres. Glass and carbon fibres were incorporated at identical dosages of 0.12%, 0.22%, and 0.43% fibre volume fraction (V_f) to enable direct comparison of their performance. The experimental investigation involved a comprehensive characterization of the concrete mixes. Fresh properties were evaluated via slump tests, while hardened properties were determined through compressive and split tensile strength testing. Durability was subsequently assessed by measuring the rate of water absorption, bulk density, and moisture content. Following this material characterization, a cradle-to-gate Life Cycle Assessment (LCA) was conducted to quantify the embodied carbon and energy. Finally, an evaluation of a novel Carbonic Anhydrase (CA)-based self-healing treatment on pre-cracked, optimised fibre-reinforced specimens was conducted. The findings highlight key performance trade-offs associated with fibre reinforcement. Although both fibre types reduced compressive strength, they markedly improved split tensile strength for glass fibres by up to 70% and carbon fibres by up to 35%. Durability responses diverged: glass fibres increased water absorption, while carbon fibres reduced water absorption at low doses, indicating reduced permeability. LCA showed a significant rise in environmental impact, particularly for carbon fibres, which increased embodied energy by up to 141%. The CA enzymatic solution enhanced crack closure in fibre-reinforced specimens, achieving up to 30% healing in carbon fibre composites. These findings suggest that fibre-reinforced enzymatic self-healing concrete offers potential for targeted high-durability applications but requires careful life-cycle optimisation.

Keywords: enzyme (Carbonic Anhydrase); life cycle assessment (LCA); self-healing concrete; durability; carbon fibre; glass fibre

Academic Editor: Salvatore Verre

Received: 11 August 2025
Revised: 15 September 2025
Accepted: 19 September 2025
Published: 24 September 2025

Citation: Rabie, M.; Bahadori-Jahromi, A.; Shaaban, I.G. Optimisation of Glass and Carbon Fibre-Reinforced Concrete with External Enzymatic Self-Healing: An Experimental and Environmental Impact Study. *Buildings* **2025**, *15*, 3455. https://doi.org/10.3390/buildings15193455

1. Introduction

The deterioration of concrete infrastructure is a pressing global issue, necessitating significant investment in inspection and maintenance [1,2]. However, conventional repair methodologies are often constrained by high costs, labour intensity, and logistical challenges, such as the accessibility of the damaged area or the need for continuous structural service [3–6]. In this context, smart materials capable of autonomic repair, or self-healing,

present a highly attractive solution for enhancing the durability and service life of concrete structures [7]. As the field has matured, a variety of verification methods, including mechanical tests, durability assessments, and microstructural analysis, have been established to quantify the efficacy of these innovative systems [8,9]. In addition, fibre reinforcement has emerged as a critical technology in modern concrete design, primarily aimed at overcoming the material's intrinsic low tensile strength and poor fracture toughness.

The incorporation of glass and carbon fibres is a well-established method for enhancing concrete's mechanical properties and durability by bridging micro-cracks to inhibit their propagation, thereby improving ductility and tensile and flexural strength [10,11]. Carbon fibre-reinforced concrete (CFRC) is particularly noted for its superior strength and resistance to environmental degradation due to the fibre's high tensile strength and corrosion resistance [12,13]. While glass fibre-reinforced concrete (GFRC) also enhances tensile performance and impact resistance, its effect on compressive strength is generally less pronounced [14–16]. The widespread use of these fibres is driven by their high strength-to-weight ratios and chemical resistance, with glass often favoured for its cost-effectiveness and carbon specified for demanding applications requiring maximum durability and mechanical performance compared to other fibres [17].

Self-healing mechanisms in concrete are broadly classified into physical, chemical, and biological processes. While physical and chemical methods have shown promise, biological approaches, particularly Microbial-Induced Carbonate Precipitation (MICP), have garnered substantial attention [18,19]. This technique utilizes bacteria to induce the precipitation of calcium carbonate ($CaCO_3$), effectively sealing cracks [20]. Research has consistently shown that the performance of MICP can be significantly enhanced by incorporating fibre reinforcements, such as polypropylene or basalt fibres. The fibres serve a dual purpose: they control the width of cracks as they form and provide nucleation sites that facilitate the deposition of the healing products directly within the crack, as illustrated in Figure 1 [21–24].

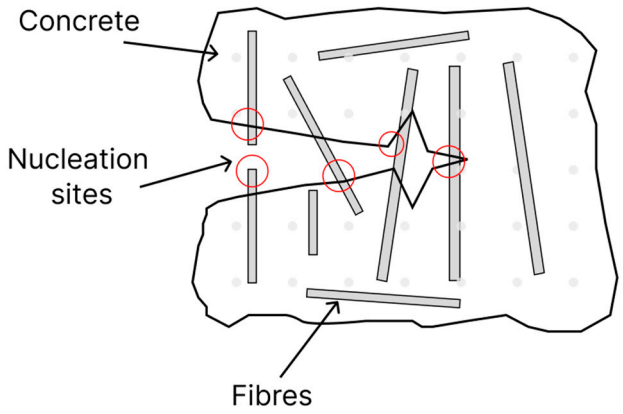

Figure 1. Fibres mediating crack control and nucleation sites for self-healing.

While MICP is a well-established technique, recent research has begun to explore alternative bio-inspired methods to overcome potential limitations such as slow reaction rates and the viability of bacteria in the highly alkaline concrete environment [25,26]. One of the most novel of these alternatives involves the use of the enzyme Carbonic Anhydrase (CA) [27,28]. This enzyme, found in all living organisms, including humans, rapidly catalyses the hydration of CO_2 to form carbonate ions, which then react with calcium ions to precipitate $CaCO_3$. This enzymatic pathway may offer a faster, more stable, and potentially more cost-effective route to biomineralization compared to cell-based systems [28]. In addition, enzymatic self-healing using CA-based approach also

offers environmental benefits, as the mineralization process absorbs atmospheric CO_2 and does not produce harmful byproducts [29]. The self-healing mechanism investigated in this study is predicated on the catalytic action of the enzyme Carbonic Anhydrase (CA). When a crack is exposed to atmospheric CO_2 and moisture, the CA enzyme rapidly catalyzes the reaction between these elements and the free calcium ions (Ca^{2+}) inherent in the cementitious matrix. This process yields the precipitation of calcium carbonate ($CaCO_3$) crystals, which possess thermomechanical properties similar to concrete hydrated products, allowing for strong interfacial bonding [28]. While a few initial studies have explored the application of Carbonic Anhydrase (CA) for the self-healing of cementitious mortar [28,30], its efficacy and influence within full concrete systems remain largely unexplored.

Building on this promising enzymatic approach to cementitious mortar, the present study investigates a novel combination of an external Carbonic Anhydrase-based healing solution with high-performance concrete reinforced with either glass or carbon fibres. A critical aspect often overlooked in the early stages of material development is a quantitative assessment of environmental performance. Given the increasing emphasis on sustainability in construction, evaluating the embodied carbon and energy of fibre-reinforced concrete is essential. While fibres can significantly enhance mechanical and durability performance, their production and incorporation may also alter the environmental profile of the composite. Systematic assessment therefore provides critical insight into the trade-offs between improved performance and environmental impact, addressing a gap that remains underexplored in the current literature. Therefore, this investigation integrates a cradle-to-gate life cycle assessment (LCA) to evaluate the embodied carbon and energy of these advanced composites, providing a more holistic understanding of their sustainability.

Accordingly, the aim of this research is to provide a comprehensive evaluation of the performance of glass and carbon fibre-reinforced concrete, both in its material properties and its capacity for enzymatic self-healing. This is achieved by (1) assessing the fresh, hardened, and durability properties of the composites; (2) quantifying their environmental footprint via an LCA; and (3) measuring the efficacy of the external enzymatic treatment on pre-cracked specimens.

2. Research Significance

The significance of this research lies in its multi-faceted investigation of a novel enzymatic self-healing technique for fibre-reinforced concrete. This study is among the first to explore the synergistic effects of an external Carbonic Anhydrase solution when applied to concrete reinforced with high-performance glass and carbon fibres. Moving beyond a singular focus on healing efficacy, the research provides a comprehensive assessment that balances mechanical performance, durability characteristics, and, crucially, the environmental footprint through a life cycle assessment. By elucidating the complex trade-offs between these properties, this work offers valuable insights for the development of advanced, resilient, and more sustainable cementitious composites.

3. Materials and Methods

3.1. Materials

This study utilised Ordinary Portland Cement (OPC) CEM II/A-L 32.5 R with a relative density of 2.75–3.20 g/cm^3 and a chemical composition shown in Table 1, conforming to BS EN 197-1 [31]. The coarse aggregate consisted of natural stone with a maximum particle size of 10 mm, retained on a 4 mm sieve. Natural sand was employed as the fine aggregate, with particles sized 4 mm and below. Prior to use, the fine aggregate was air-dried. Figure 2 shows the particle size distribution for coarse and fine aggregates. Table 2 shows the specific gravity, water absorption, and fineness modulus in accordance with the BS 812 [32]

and ASTM C33 [33]. It is worth noting that the gradation and aggregate characteristics conform to the mentioned specifications. All constituent materials, including the cement and aggregates, were procured from Travis Perkins (Northampton, UK) [34]. Potable tap water was used for both the mixing and subsequent curing of all test specimens.

Table 1. Chemical composition of Portland Cement CEM II/A-L 32.5 R.

Component	Content (%)
Cao	66.3
SiO_2	21.1
Cao/SiO_2	3.1
Al_2O_3	4.9
Fe_2O_3	2.7
MgO	1
SO_3	2.6
Loss on Ignition	5.5
Insoluble Residue	2.3

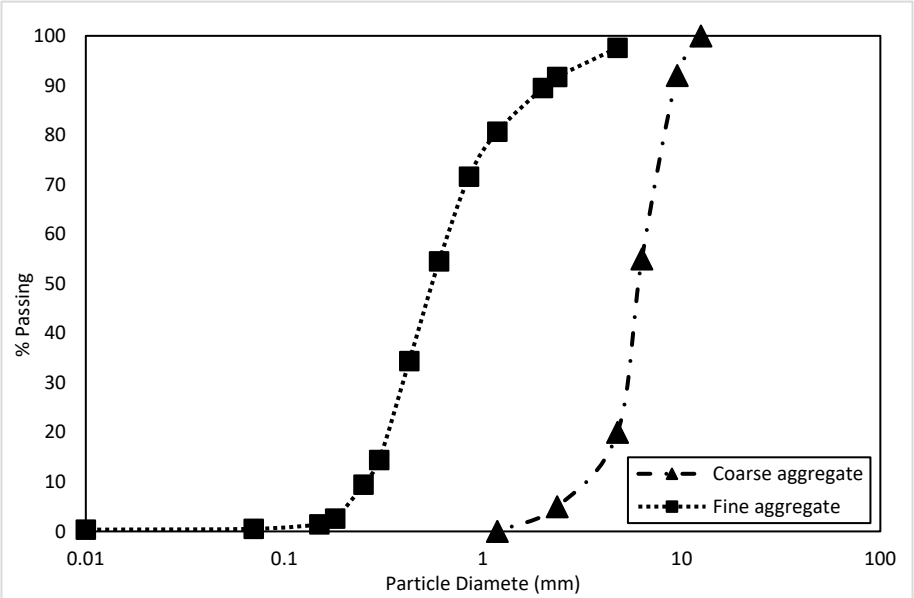

Figure 2. Particle size distribution of coarse and fine aggregates used in this study.

Table 2. Coarse and fine aggregate details.

	Coarse Aggregate	Fine Aggregate
Specific Gravity	2.54	2.62
Water Absorption (%)	1.7	2.65
Fineness Modulus	-	2.59

For this research, Alkali-Resistant Glass Fibre (GF) was sourced from Oscrete Construction Products, while Carbon Fibre (CF) was supplied by Cristex Composite Materials. Both fibres were of commercial grade and selected for their suitability in concrete applications. The general fibre properties are summarised in Table 3.

Table 3. Glass and carbon fibre properties.

Fibre Type	Glass	Carbon
Specific Gravity (g/cm^3)	2.68	1.75–1.8
Fibre Length (mm)	12	12
Fibre Diameter (μm)	19	7
Modulus of Elasticity (GPa)	72	230
Tensile Strength (MPa)	1700	4100
Softening Point (°C)	860	-

The enzymatic self-healing solution was prepared from three components as illustrated in Figure 3, following the procedure of Rosewitz et al. (2021) [28]. The Human Carbonic Anhydrase (CA) enzyme was obtained from Abbexa Ltd. (Cambridge, UK), supplied in a glass vial containing 10 μg in liquid form. The enzyme was expressed in an E. coli host and purified to approximately 95% using standard chromatographic techniques. The CA enzyme was mixed with 100 mL de-ionized water to get a concentration of 100 μg/L. A 2 M Calcium Chloride ($CaCl_2$) solution was prepared by dissolving $CaCl_2$ powder in de-ionized water. The final component was a 0.1 M Tris Buffer solution with a PH of 7.4 was procured from Sigma-Aldrich (Saint Louis, MO, USA) to maintain a relatively constant PH value.

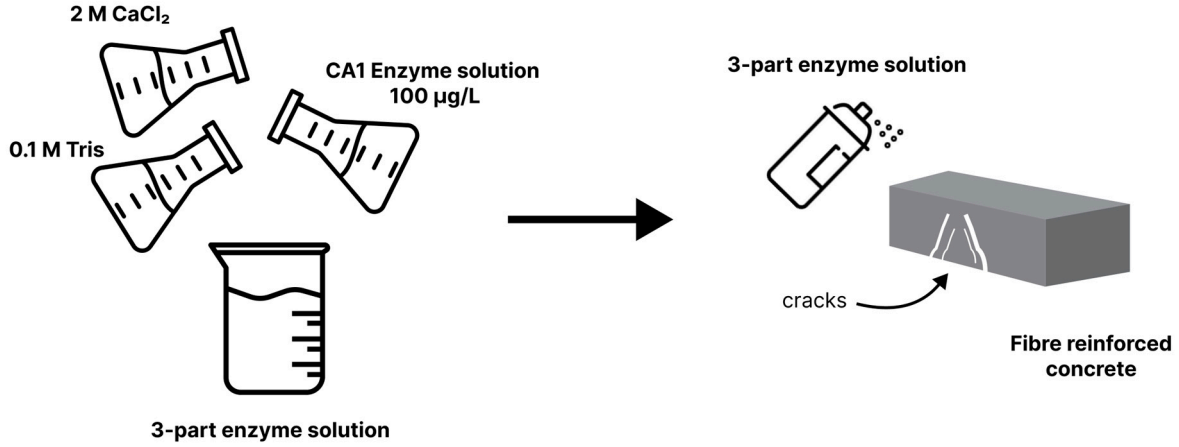

Figure 3. Carbonic Anhydrase (CA) enzymatic self-healing preparation and application.

3.2. Mix Proportions

Concrete mix design of characteristic strength 30 MPa was considered in this study. A total of seven mixes were prepared; the control mix was made of cement, water, coarse aggregates, and fine aggregates. The water–cement ratio was maintained at 0.4 for all design mixes in this investigation. Three percentages of glass and carbon fibre were examined: G1/C1 with 0.75% by cement weight (equivalent to a 0.12% fibre volume fraction (V_f)), G2/C2 with 1.32% by cement weight (0.22% V_f), and G3/C3 with 2.63% by cement weight (0.43% V_f). The specific fibre percentages were selected to address a gap in the existing literature, as a comprehensive review revealed no prior investigations into these particular volume fractions. In addition, preliminary trial mixes indicated that these percentages offered an optimal balance between mechanical performance and workability, avoiding excessive fibre clustering or segregation. The details of the mix design are depicted in Table 4.

Table 4. Details of fibrous concrete mix design.

Mix ID	Cement (Kg/m^3)	Fine Aggregate (Kg/m^3)	Coarse Aggregate (Kg/m^3)	W/C	Water	Fibre Amount (Kg/m^3)
Control	440	752	1158	0.4	176	0
G-1	440	752	1158	0.4	176	3.3
G-2	440	752	1158	0.4	176	5.808
G-3	440	752	1158	0.4	176	11.572
C-1	440	752	1158	0.4	176	3.3
C-2	440	752	1158	0.4	176	5.808
C-3	440	752	1158	0.4	176	11.572

An enzymatic self-healing solution with a total volume of 300 mL was prepared by mixing its three constituent components. The solution was formulated by combining the Human Carbonic Anhydrase (CA) solution, the 2 M $CaCl_2$ solution, and the 0.1 M Tris Buffer solution in a 1:1:1 volumetric ratio. Subsequently, the prepared enzymatic solution was applied to pre-cracked concrete beams reinforced with glass and carbon fibres to evaluate the potential of the proposed external self-healing technique.

3.3. Experimental Procedure

The mixing procedure was initiated by thoroughly combining the coarse and fine aggregates. Subsequently, either glass or carbon fibres were gradually introduced to create a homogeneous blend; this particular mixing sequence conforms to ACI 544.4R-18 [35]. Following this, cement was added, and water was introduced incrementally until a uniform and consistent mix was achieved, as shown in Figure 4. The workability of the fresh concrete was then evaluated using a slump test. The optimal percentage of glass and carbon fibres was determined based on achieving the highest split tensile strength; these optimised mixes were then selected for further evaluation of the external self-healing technique.

3.3.1. Fresh Properties

The slump test was carried out in accordance with the guidelines outlined in BS EN 12350–2:2009 [36]. Following the placement of the concrete mixtures into the designated moulds, mechanical vibration was applied to expel entrapped air and to assist in the compaction of mixes. Subsequently, the specimens remained in their steel moulds for an initial 24-hour period under controlled laboratory conditions to allow for preliminary setting.

3.3.2. Hardened Properties

The compressive strength testing procedure adopted in this study conformed to the specifications set out in BS 1881: Part 116:1983 [37]. Standard concrete cube specimens measuring 150 mm × 150 mm × 150 mm were utilised, with a total of six samples prepared for testing at two distinct curing intervals for each mix design: 7 and 28 days. Following 24 h of casting, the specimens were demoulded and subsequently immersed in a water curing tank to facilitate hydration under controlled lab conditions. Compressive strength measurements were undertaken at the respective 7-day and 28-day curing durations as shown in Figure 5a.

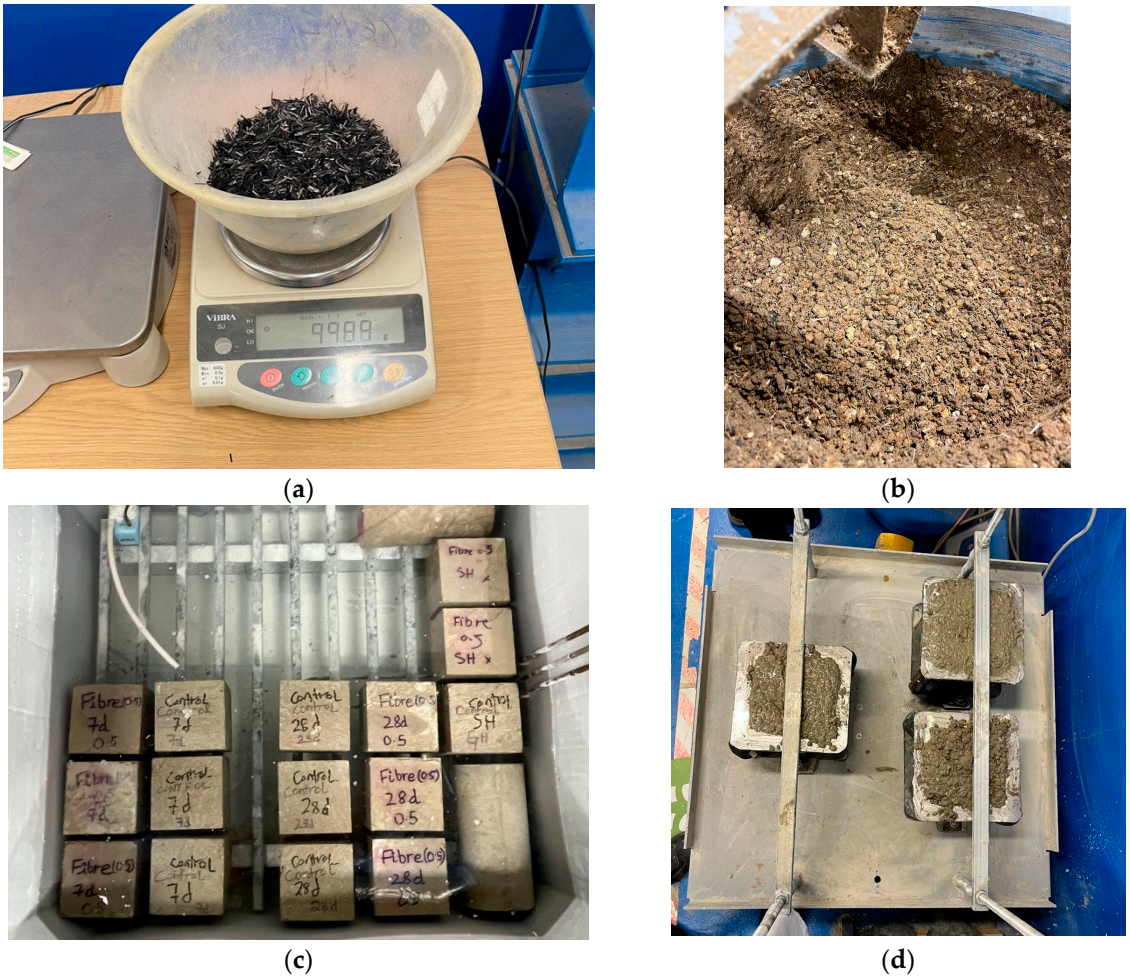

Figure 4. Mixing and preparations of concrete mixes: (**a**) Weighing of fibres; (**b**) Mixing of aggregates and fibres; (**c**) Curing of concrete specimens; (**d**) Removing the air bubbles from the casted concrete.

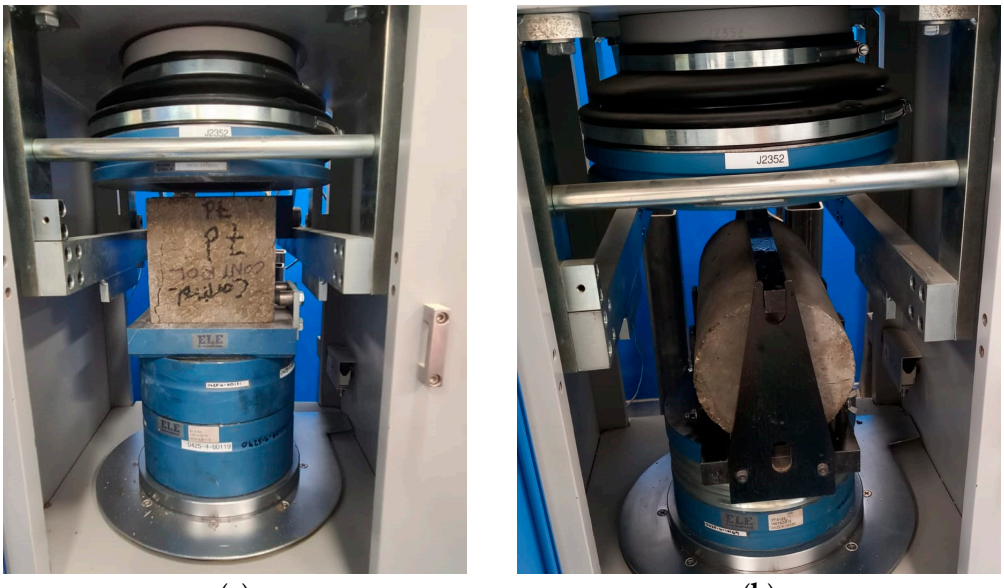

Figure 5. Mechanical testing of concrete: (**a**) Compressive strength testing, (**b**) Split tensile strength testing.

The splitting tensile strength assessment was performed in accordance with ASTM C 496 [38], employing a Universal Testing Machine with a loading capacity of 3000 kN. Cylindrical concrete specimens, each with a diameter of 150 mm and a height of 300 mm, were tested following a 28-day water curing regime as shown in Figure 5b.

3.3.3. Rate of Water Absorption

Capillary water absorption measurements were conducted on concrete cubes following oven drying at 110 °C for 24 h. After cooling to ambient laboratory temperature, the specimens were positioned on metal rods within water-filled containers to ensure unobstructed contact between the inflow surface and water, as illustrated in Figure 6. The water level was maintained at approximately 5 mm above the base of the specimens to limit hydrostatic pressure. To facilitate unidirectional water flow, the lower portions of the lateral surfaces were coated with a thin layer of grease, as shown in Figure 6. Cumulative water uptake was determined by recording the mass of each specimen at specific time intervals over a period of up to seven days, with excess surface water gently removed using a dampened tissue prior to weighing.

Figure 6. Rate of water absorption test.

3.3.4. Bulk Density

To evaluate the bulk density, three concrete cube specimens each measuring 150 mm × 150 mm × 150 mm were prepared for each mix design. The specimens were oven-dried at 110 °C for 24 h to ensure complete moisture removal. Following the drying phase, the cubes were cooled to ambient laboratory temperature for two hours before their oven-dry weights were recorded. Bulk density was determined by dividing the dry mass of each cube by its corresponding volume. The mean bulk density for each mix was then obtained by averaging the calculated densities of the three specimens.

3.3.5. Moisture Content

Moisture content is a critical parameter influencing the durability and mechanical performance of concrete. To assess this property, specimens were extracted from the curing tank and their surfaces were gently dried using a cloth to remove excess water. The wet weight of each specimen was then measured. Moisture content was subsequently determined by comparing the wet weight with the corresponding oven-dry weight obtained previously to calculate the retained moisture.

3.3.6. Enzymatic Self-Healing Procedure

The enzymatic self-healing solution prepared in Section 3.1 was applied to control specimens and to the optimised glass and carbon fibre concrete samples that exhibited the highest split tensile strength, as illustrated in Figure 3. Fibre-reinforced specimens were selected based on the principle that fibres can act as nucleation sites, thereby aiding the precipitation of calcium carbonate within the cracks [21,30,39–41]. To induce cracking, three concrete beams with dimensions of 150 mm × 150 mm × 750 mm were subjected to a three-point loading setup in a universal testing machine at a loading rate of 0.1 mm/s and a maximum load of 25 kN, as shown in Figure 7. The load was applied gradually until visible cracks of varying sizes formed; however, the test was terminated prior to the complete failure of the specimen. This pre-cracking procedure was designed to mimic an in situ repair scenario on existing structural members [42]. The enzymatic solution was subsequently applied to both small and large cracks using a spray bottle until the cracks were filled, as shown in Figure 7c. The healing process was monitored using a manual portable crack detection microscope (ELE International, Milton Keynes, UK, ×40 magnification, measuring range: 4 mm with 0.02 mm divisions) [43]. For each specimen, two cracks were selected for evaluation, as illustrated in Figure 7d.

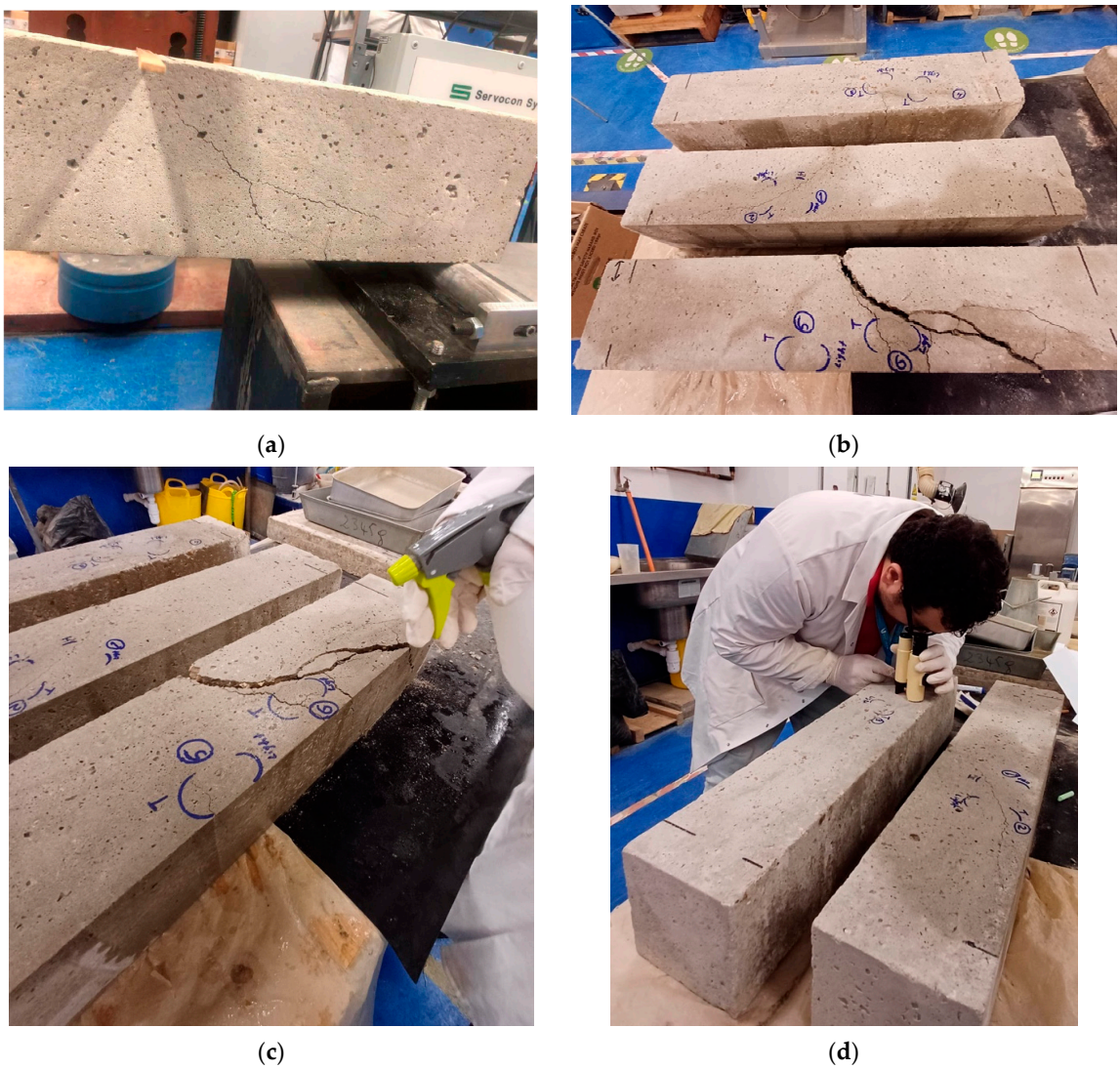

Figure 7. Application of enzymatic self-healing: (**a**) Controlled cracking of beams, (**b**) Concrete beams with various crack sizes, (**c**) Spraying the concrete beams with self-healing solution, (**d**) Measuring the healing potential using a microscope.

To quantify the healing potential over time, three readings were recorded for each crack at intervals of 0, 7, 28, and 56 days. Healing efficiency was evaluated based on the percentage of crack width closure, as calculated using Equation (1).

$$\text{HP}\ (\%) = \left(\frac{\text{CW}_\text{t} - \text{CW}_\text{i}}{\text{CW}_\text{i}}\right) \times 100 \quad (1)$$

where

- HP = Healing Percentage (%);
- CW_t = Crack Width at time t (mm);
- CW_i = Initial Crack Width (mm).

3.4. Life Cycle Assessment

A Life Cycle Assessment (LCA) is a standardized methodology used to evaluate the potential environmental impacts of a product throughout its lifecycle, from raw material extraction to final disposal [44–47]. Governed by the ISO 14044 standard [48], the process involves defining the goal and scope of the assessment, which can range from a "cradle-to-gate" (A1–A3) to a full "cradle-to-grave" analysis as illustrated in Figure 8. This is followed by the creation of a Life Cycle Inventory (LCI), which involves collecting data on all inputs and outputs for the product system, such as material quantities and embodied carbon factors. A Life Cycle Impact Assessment (LCIA) then evaluates the magnitude and significance of these environmental impacts. The process concludes with a Life Cycle Interpretation, where the findings from the LCI and LCIA are analyzed to provide recommendations and support decision-making, particularly for reducing the embodied carbon in sectors such as building and construction [49–51].

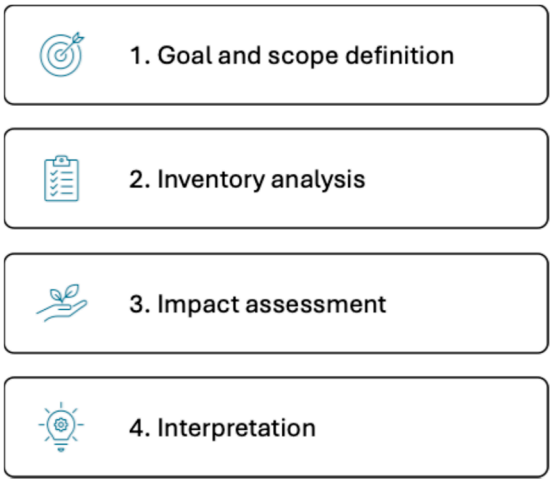

Figure 8. The four phases of life cycle assessment.

3.4.1. Goal and Scope Definition

This study aims to evaluate the environmental impacts associated with the production of 1 m^3 for each of seven distinct concrete mix designs. The assessment encompasses a control concrete mix, along with three different percentages of both carbon and glass fibre reinforcement. The analysis was conducted using a cradle-to-gate (A1–A3) system boundary, which, in accordance with ISO 14044, includes the stages of raw material supply, transport, and manufacturing up to the factory gate. It is worth noting that LCA of the enzymatic self-healing solution was not performed, as there was no data in the literature regarding the environmental impacts of the Human Carbonic Anhydrase (CA) enzyme. Therefore, it was excluded from the scope of the study.

3.4.2. Life Cycle Inventory (LCI)

The Life Cycle Inventory (LCI) phase of this study consisted of collecting two primary sets of input data: the quantities of constituent materials and their corresponding embodied carbon and energy factors. The specific material weights were derived directly from the experimental mix designs developed in this investigation. For this analysis, environmental impact factors were sourced from the Inventory of Carbon and Energy (ICE) database [52]. Originally developed by Hammond and Jones (2008) and subject to regular updates, the ICE database is a widely recognized and robust source for calculating embodied carbon and energy in the UK [53].

A summary of the embodied carbon and energy factors for all materials used in the production of the glass and carbon fibrous concrete is presented in Table 5.

Table 5. Embodied carbon and energy factors for the fibrous concrete.

Component/Material	ECF (kg CO_2e/kg)	EEF (MJ/kg)
Portland Cement (CEM I)	0.840	5.5
Fine Aggregate (Sand)	0.0048	0.081
Coarse Aggregate (Gravel)	0.0048	0.083
Water	0.001	0.01
Glass Fibre	8.1	100
Carbon Fibre	10	315

3.4.3. Interpretations of Embodied Carbon Factor and Embodied Energy

Embodied energy is formally defined as the total energy consumed during the production of a product, a scope which encompasses raw material extraction, transportation, and the manufacturing process. The embodied carbon is subsequently determined by quantifying the greenhouse gas (GHG) emissions associated with this energy consumption, which are then converted to their carbon dioxide equivalent (CO_2e) [49–51].

The embodied carbon for the constituent materials was calculated using Equation (2):

$$\text{Total Embodied Carbon} = \sum_{i=1}^{n} (\text{ECF}_i \times \text{Q}_\text{i}) \quad (2)$$

where

- ECF_i = Embodied Carbon Factor of material i (in kgCO_2e per kg);
- Q_i = Quantity of material i (in kg);
- n = Total number of different materials or components.

4. Results and Discussion

4.1. Experimental Work

4.1.1. Fresh Properties

The workability of the seven concrete mixes was evaluated using the slump test, as shown in Figure 9. The plain concrete (control) mix exhibited a slump of 60 mm, which served as the baseline for comparison against the fibre-reinforced specimens.

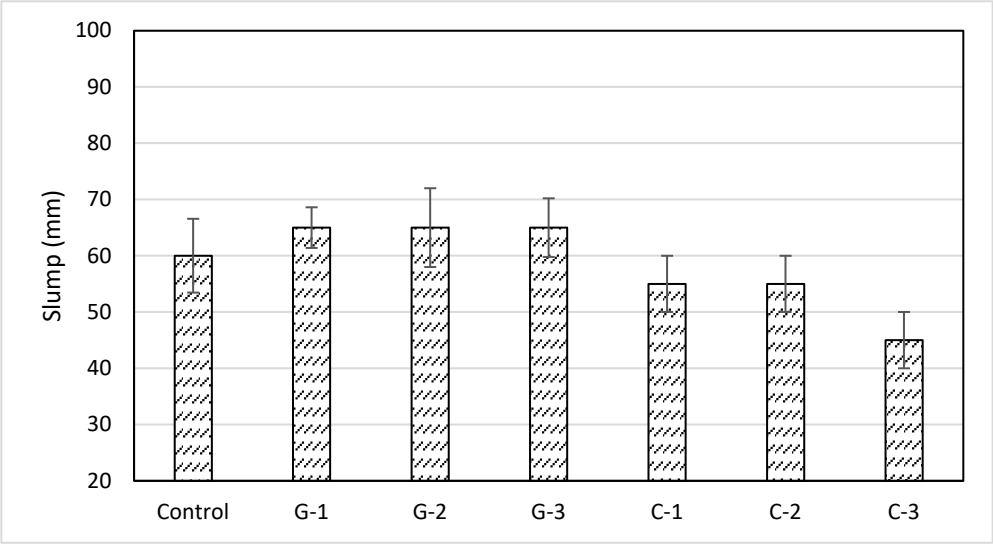

Figure 9. Slump test results for plain and fibrous concrete.

For the glass fibre concrete (GFC) series, the addition of fibres at all tested volume fractions (0.12%, 0.22%, and 0.43%) resulted in a consistent slump value of 65 mm. This uniform increase suggests that the inclusion of glass fibres provides a slight but stable enhancement in workability within the tested range. This slight increase suggests that the smooth surface and stiffness of glass fibres promote better dispersion and reduce inter-particle friction, thereby slightly enhancing workability. Similar positive effects at low fibre contents have been reported in the literature [17]. In contrast, the carbon fibre concrete (CFC) mixes displayed a different trend. The slump values for the C-1 and C-2 mixes, containing 0.12% and 0.22% carbon fibres, respectively, were identical at 55 mm. This represents a marginal decrease in workability compared to the control mix. However, a further increase in carbon fibre content to 0.43% (C-3) led to a more pronounced reduction in slump, which declined to 45 mm.

These findings indicate a notable divergence in the effects of the two fibre types on the fresh properties of the concrete. While the addition of glass fibres up to 0.43% appears to consistently and modestly improve workability, carbon fibres seem to introduce a progressive reduction in the fluidity of the mix as their concentration increases [54]. This suggests that the workability of concrete may be more sensitive to the dosage of carbon fibres than to that of glass fibres [15]. This can be attributed to the finer morphology and greater interlocking tendency of carbon fibres, which restricts the flow of the fresh mix more than glass fibres and results in reduced slump. Since both fibre types are essentially non-absorbent, the variation is instead linked to fibre distribution and dosage, as higher carbon fibre contents intensify inter-fibre friction and entanglement [55].

4.1.2. Hardened Properties

The hardened properties of the concrete were evaluated by measuring the compressive and split tensile strengths. The results indicate that the inclusion and type of fibre significantly influenced the mechanical performance of the concrete, as shown in Figure 10.

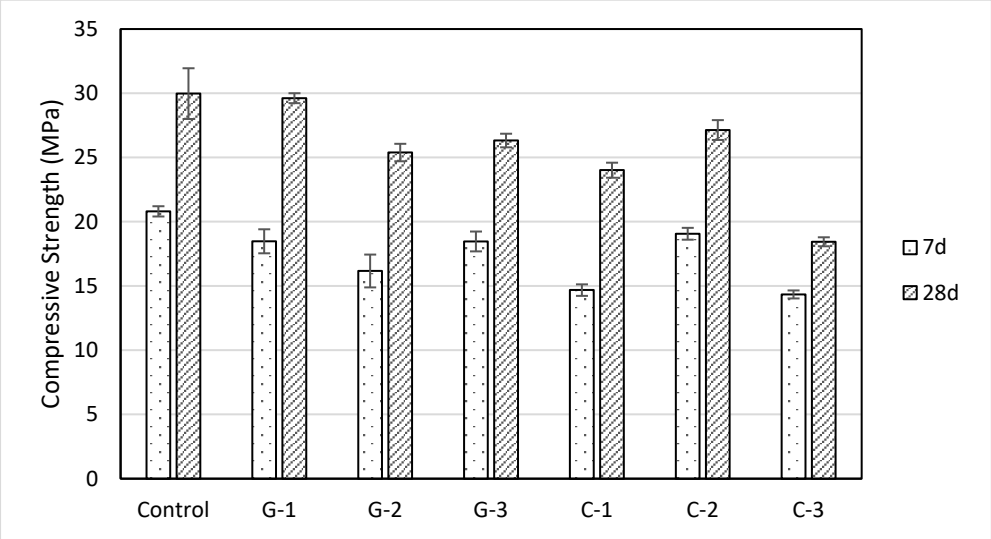

Figure 10. Compressive strength of control, glass, and carbon fibre concrete at 7 and 28 days.

The influence of fibre inclusion on compressive strength was evaluated at 7 and 28 days. The control specimen, without any fibre reinforcement, established baseline strengths of 20.81 MPa and 29.97 MPa at 7 and 28 days, respectively. The addition of glass fibres (GFC) generally resulted in a reduction in compressive strength. This effect was most pronounced in the G-2 mix (0.22% fibres), which recorded a 15% decrease in 28-day strength to 25.39 MPa. The G-1 mix (0.12% fibres), however, showed a minimal impact with only a 1% reduction at 28 days, when compared with the control mix. A more significant detrimental effect was observed with the inclusion of carbon fibres (CF). In general, CFC mixes exhibited lower compressive strengths than their GFC counterparts at equivalent dosages, although at the 28-day age, C-2 showed a marginally higher strength than G-2. The most substantial impairment was noted in the C-3 mix (0.43% fibres), which yielded a 28-day strength of only 18.44 MPa, a 38% reduction from the control. These results suggest that while both fibres impair compressive performance, the effect appears to be more severe with carbon fibres, particularly at higher concentrations.

In contrast to the compressive strength results, the inclusion of both fibre types had a positive effect on the split tensile strength, as shown in Figure 11. The control mix exhibited a baseline tensile strength of 2.00 MPa. A substantial enhancement was observed in the GFC series, which peaked with the G-2 mix (0.22% fibres). This mix achieved a tensile strength of 3.41 MPa, representing a 70% improvement over the control.

The carbon fibres also improved tensile performance, though to a lesser extent. The optimal dosage for carbon fibres was similarly found at 0.22% (C-2), which yielded a tensile strength of 2.71 MPa (a 35% increase). This indicates that while both fibres enhance tensile capacity, peaking at an equivalent fibre content, the glass fibres provided a significantly greater performance benefit at the optimal concentration in this study.

The divergent performance of fibre-reinforced concrete under compressive and tensile loading may be attributed to the fundamental mechanics of the composite material. Under tensile stress, the fibres can effectively bridge micro-cracks as they form, arresting their propagation and transferring stress across the fractured plane. This mechanism enhances the overall tensile capacity of the concrete [56,57].

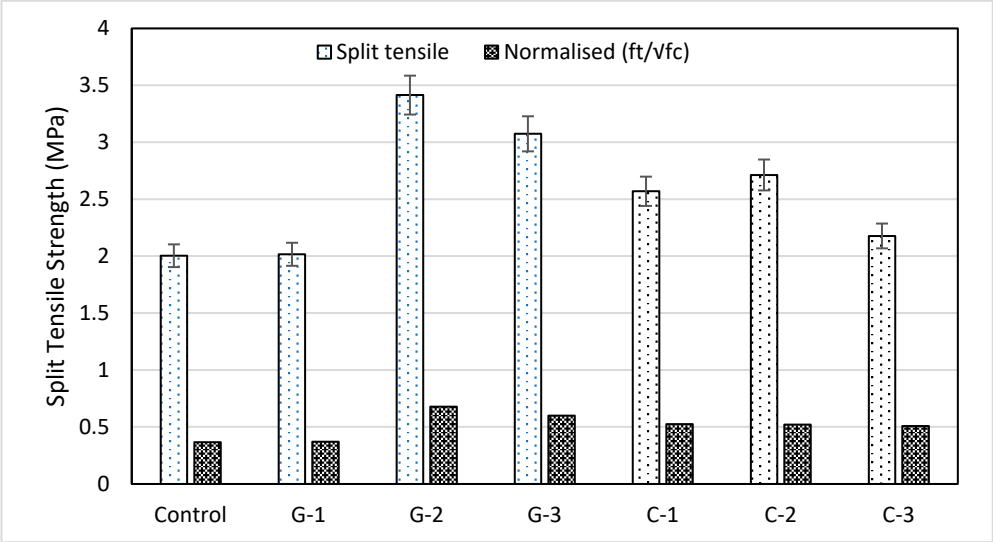

Figure 11. Split tensile strength of control, glass and carbon fibre at 28 days.

Conversely, under compression, the fibres can act as points of internal stress concentration or create voids, which may disrupt the homogeneity of the concrete matrix and lead to a reduction in compressive strength. Strength reduction in carbon fibre-reinforced mixes could be linked to reduced workability, increased air entrapment, and poor fibre-matrix bonding, resulting in lower matrix density and mechanical performance [58]. It is also suggested that factors such as fibre orientation and the quality of the fibre-matrix bond are critical; these mechanisms are likely more effective under tensile loading, which could explain the observed performance dichotomy [59,60]. These findings align with the literature, as similar trends have been reported [61,62], who observed reduced compressive strength but improved tensile or flexural performance with carbon and glass fibre inclusion.

4.1.3. Rate of Water Absorption

The durability of the concrete mixes was assessed by measuring the rate of water absorption through a capillary test as detailed in Section 3.3.3. The results, illustrated in Figure 12, reveal divergent trends depending on the type of fibre reinforcement used.

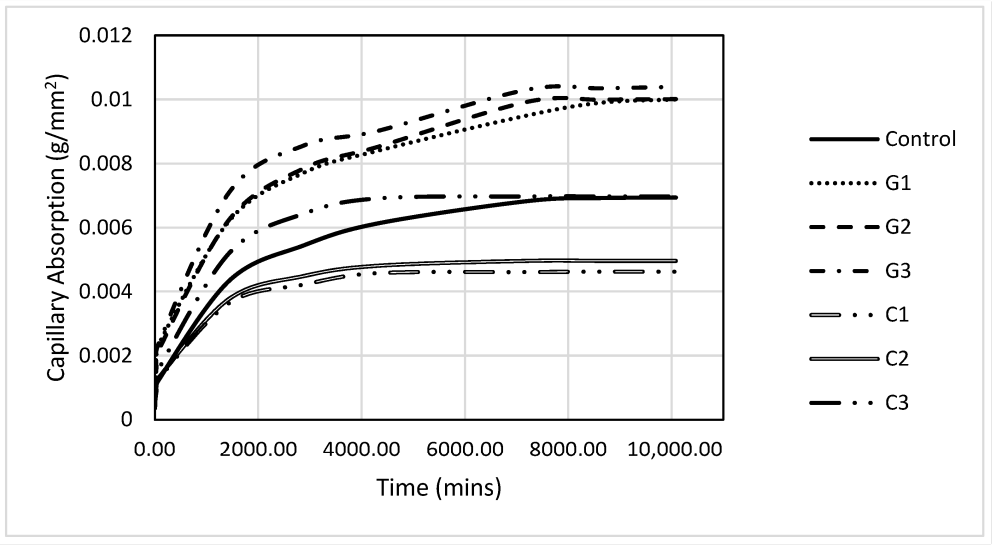

Figure 12. Rate of water absorption results for control, glass, and carbon fibre concrete.

The control specimen exhibited a gradual increase in capillary absorption over the 10,080-minute test period, reaching a final value of 0.0069 g/mm^2. This served as the baseline for evaluating the performance of the fibre-reinforced mixes. A distinct increase in water absorption was observed for all GFC mixes relative to the control. This effect was dose-dependent; the G-3 mix, with the highest fibre content (0.43%), consistently showed the highest absorption values, culminating in a final rate of 0.0104 g/mm^2. In contrast, the inclusion of carbon fibres (CF) resulted in a marked reduction in water absorption compared to the control. The C-1 mix (0.12% fibres) was particularly effective, recording the lowest absorption rate of all mixes with a final value of just 0.0046 g/mm^2. However, this benefit appeared to diminish as the fibre content increased, with the absorption rate of the C-3 mix (0.0070 g/mm^2) approaching that of the control specimen by the end of the test.

The opposing effects of the two fibre types suggest different impacts on the concrete's microstructure. The increased absorption in the GFC mixes may indicate that the inclusion of glass fibres introduces a more porous network or a less refined fibre-matrix interface, facilitating greater water ingress [63]. Conversely, the reduced permeability of the CFC mixes, especially at lower concentrations, suggests that carbon fibres may help to refine the pore structure of the concrete matrix [10,64]. These findings highlight a critical trade-off between the mechanical and durability properties of the mixes. While glass fibres provided a greater enhancement in tensile strength, they appear to compromise the material's resistance to water penetration. Carbon fibres, on the other hand, seem to improve this aspect of durability.

4.1.4. Bulk Density

The bulk density of the hardened concrete specimens was determined for each mix design, with the results shown in Figure 13. The analysis indicates that the inclusion of both fibre types generally reduces the bulk density of the concrete, though the magnitude and trend of this effect vary significantly between glass and carbon fibres.

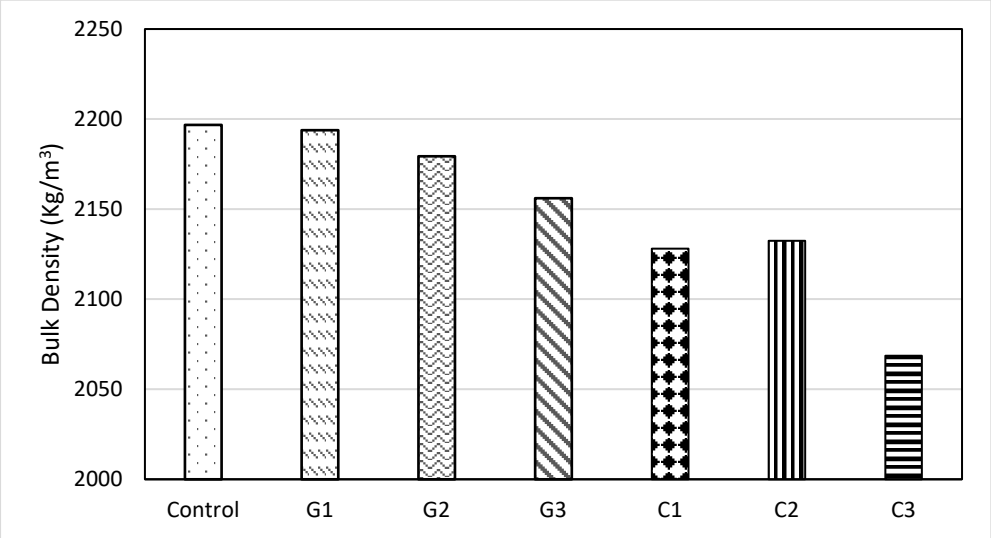

Figure 13. Bulk density results for control, glass, and carbon fibre concrete.

The control mix, containing no fibres, exhibited the highest bulk density at 2196.77 kg/m^3. For GFC series, a clear, dose-dependent decrease in density was observed. The density was reduced from 2193.81 kg/m^3 in the G-1 mix (0.12% fibres) to 2156.06 kg/m^3 in the G-3 mix (0.43% fibres). A more substantial reduction in bulk density was recorded for the CFC series. At all equivalent dosages, the CFC mixes were less dense than the GFC mixes. The C-3

mix, with 0.43% carbon fibres, had the lowest density of all specimens at 2068.56 kg/m^3. An interesting deviation from a linear trend was observed within the CFC series; the bulk density increased slightly from 2128.09 kg/m^3 for the C-1 mix to 2132.41 kg/m^3 for the C-2 mix, before declining significantly in the C-3 mix.

This general trend of decreasing density with fibre inclusion may be attributed to the lower density of the fibres themselves compared to the cementitious matrix, as well as the potential for an increased void content resulting from fibre dispersion [65–67]. The more pronounced effect of the carbon fibres is likely due to the inherently lower density of carbon fibre compared to glass fibre.

4.1.5. Moisture Content

The moisture content of the hardened concrete specimens was measured to assess the influence of fibre reinforcement, as shown in Figure 14. The analysis reveals that the inclusion of both fibre types generally increases the moisture content relative to the control specimen, though the trends differ between the two.

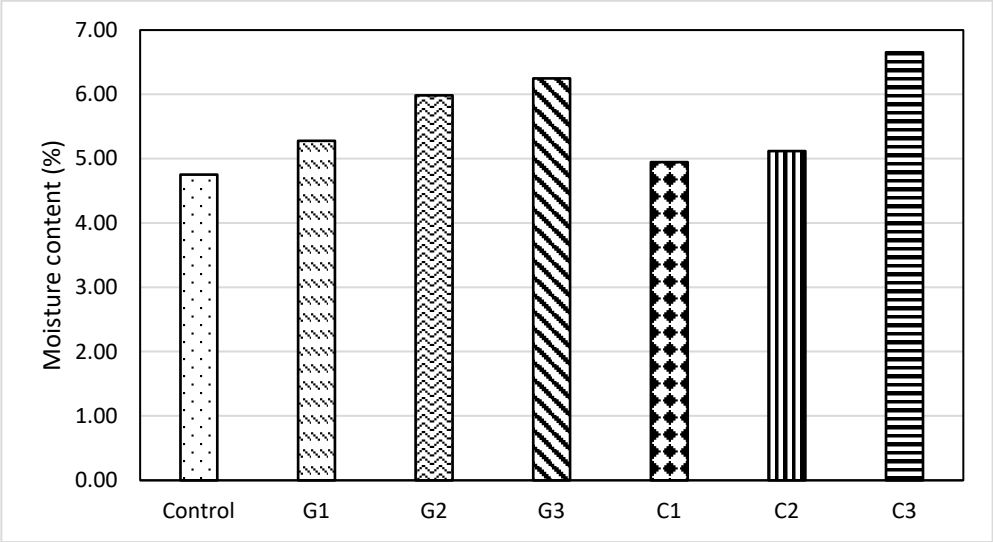

Figure 14. Moisture content results for control, glass, and carbon fibrous concrete.

The control mix established a baseline moisture content of 4.75%. For GFC series, a consistent, dose-dependent increase was observed; the moisture content rose from 5.28% in the G-1 mix to a peak of 6.25% in the G-3 mix (0.43% fibres). A similar increasing trend was noted for the CFC series. However, a direct comparison shows that at lower dosages (0.12% and 0.22%), the CFC mixes retained less moisture than their GFC counterparts. This relationship inverted at the highest dosage of 0.43%, where the C-3 mix exhibited a moisture content of 6.65%, which is the highest value recorded among all specimens.

The general increase in moisture content may be attributed to a higher porosity or a larger internal surface area introduced by the fibres, which enhances the concrete's ability to absorb and retain water [63]. The data suggest a complex interaction, where at lower concentrations, glass fibres appear to contribute more to moisture retention than carbon fibres. At higher concentrations, however, the properties of the carbon fibres seem to result in the most significant increase in the specimen's final moisture content.

4.2. Life Cycle Assessment

The life cycle assessment, constrained to a cradle-to-gate (A1–A3) boundary, quantified the embodied carbon and embodied energy for each of the seven concrete mix designs. The results indicate that the inclusion of either fibre type increases the environmental burden of

the concrete, with carbon fibres having a particularly pronounced effect. However, when normalised against the corresponding mechanical and durability improvements, carbon fibre reinforcement exhibited a higher performance-to-impact ratio for tensile strength and crack resistance than glass fibre, suggesting potential justification in applications where extended service life, reduced maintenance frequency, or superior crack control outweigh the higher embodied impacts.

4.2.1. Embodied Carbon

The analysis of embodied carbon revealed a clear, dose-dependent increase with the addition of both fibre types. The plain concrete mix established a baseline of 378.9 kg CO_2e per m^3 as shown in Figure 15. The inclusion of glass fibres led to a steady rise in embodied carbon, from a 7.1% increase for the G-1 mix up to a 24.7% increase for the G-3 mix. A similar, though slightly more impactful, trend was observed for the carbon fibre concrete. At equivalent dosages, the carbon fibre mixes consistently exhibited a higher embodied carbon than their glass fibre counterparts. This culminated in the C-3 mix (0.43% fibres) having the highest carbon footprint of all specimens at 494.6 kg CO_2e, a 30.5% increase over the control mix [14].

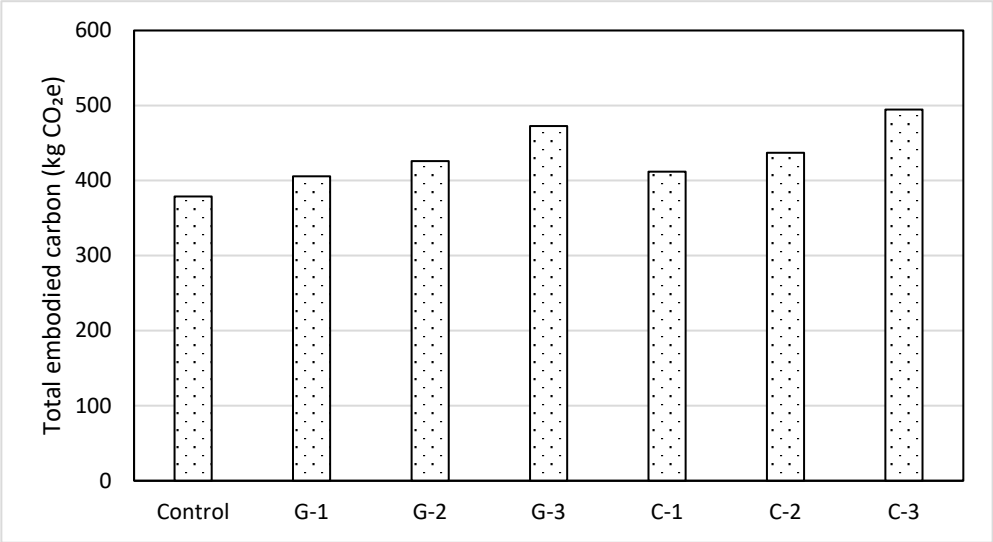

Figure 15. Total embodied carbon for different mix designs of fibrous concrete.

4.2.2. Embodied Energy

The disparity between the two fibre types was substantially more dramatic when assessing embodied energy. The control mix required 2578.8 MJ per m^3 for its production. While the glass fibre mixes also showed a dose-dependent increase, rising by up to 44.9% for the G-3 mix, the impact of the carbon fibres was an order of magnitude greater. Even the lowest dosage of carbon fibres (C-1) resulted in a 40.3% increase in embodied energy, a figure comparable to the highest dosage of glass fibres. This effect escalated sharply with concentration, with the C-3 mix requiring 6224.0 MJ—a staggering 141.4% increase over the control specimen, as shown in Figure 16.

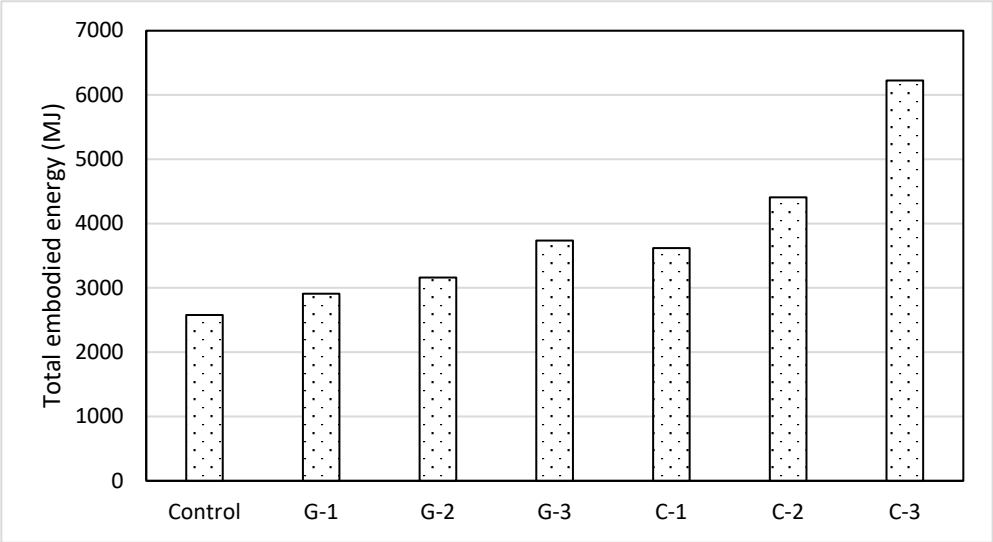

Figure 16. Total embodied energy for different mix designs of fibrous concrete.

These findings suggest that while both fibres add to the environmental footprint of the concrete, the energy-intensive nature of carbon fibre manufacturing makes it a significant driver of the overall environmental impact [68]. This presents a critical trade-off: the mechanical benefits offered by fibre reinforcement, particularly carbon fibre, appear to come at a substantial environmental cost, most notably in terms of embodied energy, which can be reduced using energy-efficient production techniques [69,70].

4.3. Enzymatic Self-Healing

The efficacy of the external enzymatic self-healing treatment was evaluated by monitoring the crack width closure over a 56-day period. The healing potential (HP), expressed as a percentage, was calculated for two cracks of varying initial widths in the control, G-2 (0.22% glass fibre), and C-2 (0.22% carbon fibre). As the G-2 and C-2 mixes exhibited the highest split tensile strength at 28 days, they were subsequently selected for the enzymatic self-healing evaluation. The results are presented in Table 6 and Figure 17.

Table 6. Crack identification with initial crack width.

Mix ID	Crack No.	Initial Crack Width (mm)	Final Crack Width (mm)
Control (#1)	1	0.48	0.4
Control (#2)	2	1.1	0.92
G-2 (#1)	3	1	0.77
G-2 (#2)	4	0.35	0.25
C-2 (#1)	5	0.34	0.245
C-2 (#2)	6	1.5	1.05

The control specimens demonstrated a modest level of autogenous healing, achieving a final healing potential of approximately 16–17% at 56 days, regardless of the initial crack width (0.48 mm or 1.1 mm). This establishes the baseline performance of the enzymatic solution on plain concrete. A significant improvement in healing was observed with the inclusion of fibres. The G-2 specimens reached a final HP of 23.00% for a 1.0 mm crack and 28.57% for a 0.35 mm crack. The highest healing performance was recorded for the C-2 specimens, which attained a final HP of 27.94% for a 0.34 mm crack and 30.00% for a wider 1.5 mm crack. These results clearly indicate that the presence of either fibre type substantially enhances the healing process compared to the control specimen.

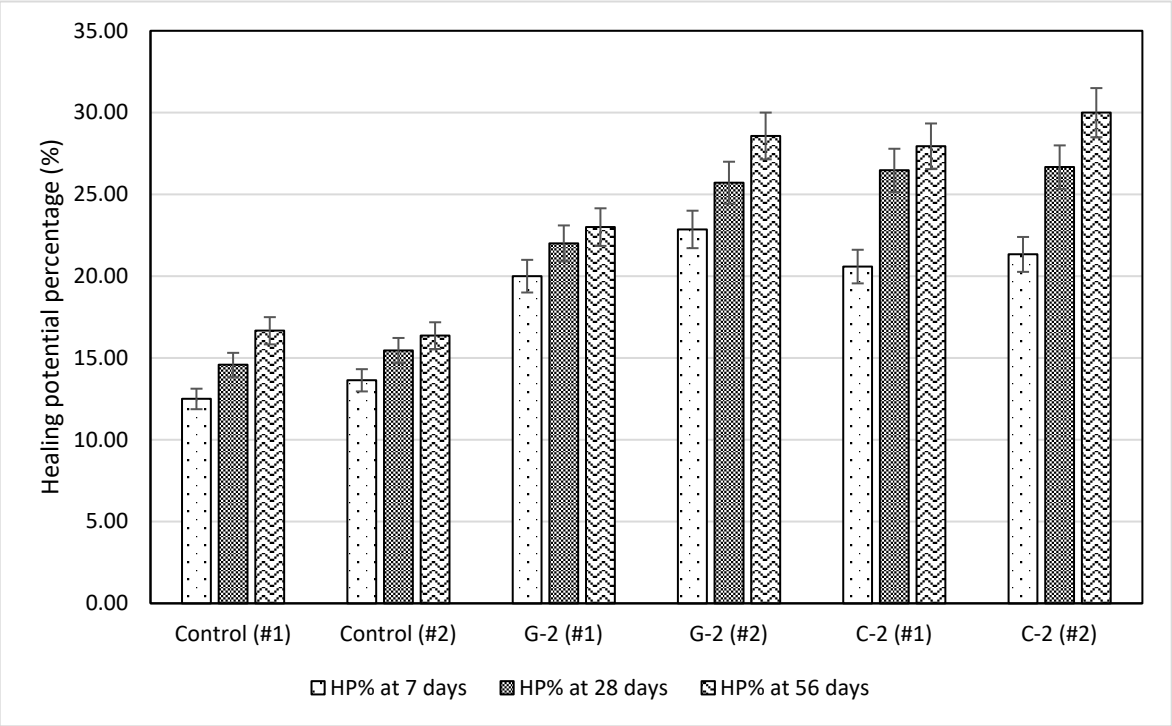

Figure 17. Healing potential of control, glass, and carbon fibre concrete.

The superior performance of the fibre-reinforced composites suggests that the fibres play a crucial role in the healing mechanism [71,72]. It is postulated that the fibres spanning the crack act as nucleation sites, providing a physical scaffold that facilitates the precipitation of calcium carbonate from the enzymatic solution. This bridging effect appears to be most pronounced in the carbon fibre specimens, which may be attributed to the surface properties of carbon providing a more favourable substrate for crystal growth compared to glass [73]. Interestingly, while the healing potential in the G-2 specimen was higher for the smaller crack, a different trend was observed for the C-2 specimen, where the wider crack healed slightly more completely. Although this specific observation may warrant further investigation, the overall results demonstrate that fibre reinforcement, and particularly carbon fibre at this dosage, significantly improves the efficacy of the external enzymatic self-healing treatment.

The crack healing capacity of the CA enzymatic self-healing solution (0.45 mm) observed in this study is comparable to microbial-based systems reported in the literature, as shown in Table 7. Its performance is slightly lower than the highest values achieved with Bacillus pasteurii combined with sisal fibre (0.80 mm) and Bacillus cohnii with expanded perlite (0.79 mm), but it is similar to Bacillus with nanoclay (0.46 mm) and Bacillus subtilis with sisal fibre (0.48 mm). Compared to other microbial carriers such as recycled aggregate (0.27 mm), PVA fibres (0.30 mm), or zeolites (0.10 mm), the CA enzymatic approach demonstrates improved healing potential. These results indicate that CA-based systems can achieve competitive healing efficiency without the biological and durability limitations often associated with microbial carriers, highlighting their promise as a practical and scalable alternative for self-healing concrete applications.

Table 7. Crack healing widths of microbial-based materials and the CA enzymatic self-healing solution (Modified from [74,75]).

Materials	Crack Healing Width (mm)	Reference
CA enzymatic solution/Carbon fibre (Present study)	0.45	–
Bacillus pasteurii/Ceramic granule	0.51	[76]
Bacillus pasteurii/Recycled aggregate	0.27	[77]
Bacillus pasteurii/Sisal fibre	0.8	[78]
Bacillus cohnii/Magnesium oxide cementitious capsules	0.25	[79]
Bacillus subtilis/Sisal fibre	0.48	[25]
Bacillus subtilis/Polyvinyl alcohol fibres	0.3	[80]
Bacillus megaterium/Zeolites	0.1	[81]
Bacillus/Nanoclay	0.46	[82]
Bacillus mucus/Expanded vermiculite	0.4	[83]

5. Conclusions

This study was conducted to comprehensively evaluate and compare the effects of incorporating varying dosages of glass and carbon fibres into concrete. The investigation encompassed an experimental analysis of the fresh, hardened, and durability properties of seven distinct concrete mixes. Furthermore, a cradle-to-gate life cycle assessment was performed to quantify the embodied carbon and energy of each mix. Finally, the efficacy of an external enzymatic self-healing technique was assessed on the mechanically optimal fibre-reinforced specimens. The principal findings of this investigation are summarised as follows:

- Both glass and carbon fibres were found to reduce the compressive strength of the concrete, with the detrimental effect being more pronounced for carbon fibres, particularly at higher concentrations. Conversely, the inclusion of both fibre types enhanced the split tensile strength, peaking at an optimal dosage of 0.22%. Glass fibres provided a significantly greater improvement (+70%) compared to carbon fibres (+35%) at this concentration.
- A critical trade-off was identified in the durability of the mixes. The addition of glass fibres consistently increased the rate of water absorption, suggesting higher permeability. In contrast, the low dosage of 0.12% carbon fibre resulted in a pronounced reduction in water absorption (33.33%) compared to the control, indicating enhanced durability.
- The life cycle assessment indicated that fibre inclusion increases the environmental footprint of the concrete. This impact was most significant for the carbon fibre mixes, which led to a substantial increase in embodied energy (up to 141%) compared to both the control and the glass fibre mixes.
- The application of an external enzymatic self-healing solution was more effective on fibre-reinforced specimens than on the plain control, suggesting that fibres act as nucleation sites. The optimal carbon fibre concrete (C-2) exhibited the highest healing potential, achieving up to 30% crack closure after 56 days, representing a 13.33% improvement over the control mix.
- The CA enzymatic self-healing solution demonstrated a crack healing capacity (0.45 mm) comparable to or exceeding several microbial-based systems, highlighting its potential as a competitive and practical alternative for self-healing concrete.

It is important to acknowledge the limitations of the present study, which naturally pave the way for future work. The self-healing results, while promising, are based on a specific enzymatic solution concentration applied to just two types of fibre reinforcement. Consequently, further experiments are certainly needed to validate and expand upon these findings. It would be particularly insightful to explore how different concentrations of the

enzymatic solution affect the healing rate and to test this technique on concrete reinforced with other common fibres, such as steel or synthetic polymers. A further, more practical limitation we faced was the inability to perform a detailed microstructural analysis due to the unavailability of the necessary equipment. Such an analysis, likely using Scanning Electron Microscopy (SEM), would have allowed for a direct visual confirmation of calcium carbonate precipitation within the cracks and a more thorough examination of the fibre-matrix interface, providing a deeper mechanistic understanding of our observations. This study did not include long-term durability tests such as freeze–thaw or chloride ion penetration, which should be addressed in future work to fully assess self-healing performance.

Looking forward, this research highlights several compelling avenues for further investigation. While much of the existing literature focuses on self-healing in newly cast concrete, there is a clear need to evaluate the effectiveness of enzymatic self-healing in existing, aged, and damaged structures, where the repair effect may differ significantly. In addition, a systematic exploration of alternative enzymatic sources could identify agents with improved efficiency, durability under alkaline conditions, and cost-effectiveness. Finally, developing and testing CA enzyme encapsulation technologies offers a promising pathway to enhance enzyme stability and ensure sustained self-healing performance in real structural applications.

Author Contributions: M.R.: Conceptualization, Formal analysis, Investigation, Methodology, Visualization, Writing—original draft, Writing—review & editing. A.B.-J.: Conceptualization, Supervision, Writing—review & editing. I.G.S.: Conceptualization, Supervision, Writing—original draft. All authors have read and agreed to the published version of the manuscript.

Funding: This work was partially funded by the UWL Vice Chancellor's Scholarship awarded to the first author.

Data Availability Statement: Data is contained within the article.

Acknowledgments: The authors gratefully acknowledge the support of Kanishka Turrakheil for his support during the mixing and testing of concrete specimens. We also extend our gratitude to Ibrahim Shaaban, who passed away during the last preparation stages of this manuscript. His legacy will always remain as a guide to his fellow scholars and students.

Conflicts of Interest: The authors declare no conflicts of interest.

Abbreviations

The following abbreviations are used in this manuscript:

CA	Carbonic Anhydrase
LCA	Life Cycle Assessment
MICP	Microbial-Induced Carbonate Precipitation
$CaCO_3$	Calcium Carbonate
OPC	Ordinary Portland Cement
GF	Glass Fibre
CF	Carbon Fibre
$CaCl_2$	Calcium Chloride
FRC	Fiber-Reinforced Concrete
LCI	Life Cycle Inventory
LCIA	Life Cycle Impact Assessment
ICE	Inventory of Carbon and Energy
GHG	Greenhouse gas
GFC	Glass fibre concrete
CFC	Carbon fibre concrete
V_f	Fibre volume fraction

References

1. Qu, F.; Li, W.; Dong, W.; Tam, V.W.Y.; Yu, T. Durability Deterioration of Concrete under Marine Environment from Material to Structure: A Critical Review. *J. Build. Eng.* **2021**, *35*, 102074. [CrossRef]
2. Faris, N.; Zayed, T.; Fares, A. Review of Condition Rating and Deterioration Modeling Approaches for Concrete Bridges. *Buildings* **2025**, *15*, 219. [CrossRef]
3. Noeiaghaei, T.; Mukherjee, A.; Dhami, N.; Chae, S.-R. Biogenic Deterioration of Concrete and Its Mitigation Technologies. *Constr. Build. Mater.* **2017**, *149*, 575–586. [CrossRef]
4. Kiani, B.; Liang, R.Y.; Gross, J. Material Selection for Repair of Structural Concrete Using VIKOR Method. *Case Stud. Constr. Mater.* **2018**, *8*, 489–497. [CrossRef]
5. Jiang, L.; Wu, M.; Du, F.; Chen, D.; Xiao, L.; Chen, W.; Du, W.; Ding, Q. State-of-the-Art Review of Microcapsule Self-Repairing Concrete: Principles, Applications, Test Methods, Prospects. *Polymers* **2024**, *16*, 3165. [CrossRef] [PubMed]
6. Ibrahim, M.; Ebead, U.; al-Hamrani, A.; Rabie, M. Influence of Steel Reinforced Grout Configuration, and Reinforcement Ratio on the Flexural Performance of Strengthened Continuous RC Beams. *Struct. Concr.* **2025**. [CrossRef]
7. Ma, C.-K.; Apandi, N.M.; Sofrie, C.S.Y.; Ng, J.H.; Lo, W.H.; Awang, A.Z.; Omar, W. Repair and Rehabilitation of Concrete Structures Using Confinement: A Review. *Constr. Build. Mater.* **2017**, *133*, 502–515. [CrossRef]
8. Kumpati, R.; Skarka, W.; Ontipuli, S.K. Current Trends in Integration of Nondestructive Testing Methods for Engineered Materials Testing. *Sensors* **2021**, *21*, 6175. [CrossRef]
9. Wang, B.; Zhong, S.; Lee, T.-L.; Fancey, K.S.; Mi, J. Non-Destructive Testing and Evaluation of Composite Materials/Structures: A State-of-the-Art Review. *Adv. Mech. Eng.* **2020**, *12*, 168781402091376. [CrossRef]
10. Raza, S.S.; Qureshi, L.A.; Ali, B.; Raza, A.; Khan, M.M. Effect of Different Fibers (Steel Fibers, Glass Fibers, and Carbon Fibers) on Mechanical Properties of Reactive Powder Concrete. *Struct. Concr.* **2021**, *22*, 334–346. [CrossRef]
11. More, F.M.D.S.; Subramanian, S. Impact of Fibres on the Mechanical and Durable Behaviour of Fibre-Reinforced Concrete. *Buildings* **2022**, *12*, 1436. [CrossRef]
12. Mohamed, O.; Zuaiter, H. Fresh Properties, Strength, and Durability of Fiber-Reinforced Geopolymer and Conventional Concrete: A Review. *Polymers* **2024**, *16*, 141. [CrossRef]
13. Ali, B.; Qureshi, L.; Shah, S.; Rehman, S.; Hussain, I.; Iqbal, M. A Step towards Durable, Ductile and Sustainable Concrete: Simultaneous Incorporation of Recycled Aggregates, Glass Fiber and Fly Ash. *Constr. Build. Mater.* **2020**, *251*, 118980. [CrossRef]
14. Tahir, H.; Khan, M.B.; Shafiq, N.; Radu, D.; Nyarko, M.H.; Waqar, A.; Almujibah, H.R.; Benjeddou, O. Optimisation of Mechanical Characteristics of Alkali-Resistant Glass Fibre Concrete towards Sustainable Construction. *Sustainability* **2023**, *15*, 11147. [CrossRef]
15. Ahmad, J.; González-Lezcano, R.A.; Majdi, A.; Ben Kahla, N.; Deifalla, A.F.; El-Shorbagy, M.A. Glass Fibers Reinforced Concrete: Overview on Mechanical, Durability and Microstructure Analysis. *Materials* **2022**, *15*, 5111. [CrossRef] [PubMed]
16. Ortiz, J.; Dolati, S.S.K.; Malla, P.; Nanni, A.; Mehrabi, A. FRP-Reinforced/Strengthened Concrete: State-of-the-Art Review on Durability and Mechanical Effects. *Materials* **2023**, *16*, 1990. [CrossRef]
17. Ruben, N.; Venkatesh, C.; Durga, C.; Chand, M. Comprehensive Study on Performance of Glass Fibers-Based Concrete. *Innov. Infrastruct. Solut.* **2021**, *6*, 112. [CrossRef]
18. Bio-Based Solutions for Concrete Infrastructure: A Review of Microbial-Induced Carbonate Precipitation in Crack Healing. Available online: https://www.mdpi.com/2075-5309/15/7/1052 (accessed on 1 August 2025).
19. Wang, R.; Bian, S.; Zhang, B.; Yan, L.; Feng, L.; Bai, J. Investigation of Microbial Induced Calcium Carbonate and Struvite Co-Precipitation on Cementitious Material Surfaces. *J. Environ. Manag.* **2025**, *375*, 124206. [CrossRef]
20. Yan, Y.; Jia, G.; Li, Z.; Liu, W.; Zhang, Y.; Ma, G.; Gao, Y. "Smart" Concrete Based on Microbially Induced Carbonate Precipitation—A Review. *Constr. Build. Mater.* **2024**, *451*, 138904. [CrossRef]
21. Wang, C.; Li, X.; Zhu, J.; Wei, W.; Qu, X.; Wang, L.; Sun, N.; Zhang, L. Microbial Culture Condition Optimization and Fiber Reinforcement on Microbial-Induced Carbonate Precipitation for Soil Stabilization. *Sustainability* **2025**, *17*, 3101. [CrossRef]
22. Zhang, D.; Shahin, M.A.; Yang, Y.; Liu, H.; Cheng, L. Effect of Microbially Induced Calcite Precipitation Treatment on the Bonding Properties of Steel Fiber in Ultra-High Performance Concrete. *J. Build. Eng.* **2022**, *50*, 104132. [CrossRef]
23. Wan, S.; Shu, Z.; Kang, S.; Zhong, W.; Zhang, X.; Wu, H.; Liu, R. Microbial-Induced Calcium Carbonate Precipitation and Basalt Fiber Cloth Reinforcement Used for Sustainable Repair of Tunnel Lining Cracks. *Buildings* **2024**, *14*, 3609. [CrossRef]
24. Rabie, M.; Shaaban, I.G. Glass Fibre Concrete: Experimental Investigation and Predictive Modeling Using Advanced Machine Learning with an Interactive Online Interface. *Constr. Build. Mater.* **2025**, *472*, 140951. [CrossRef]
25. Amjad, H.; Arsalan Khushnood, R.; Ali Memon, S. Biomimetic Robust Self-Healing of *Bacillus Subtilis* Immobilized through Sisal Fiber for next-Generation Concrete Infrastructure. *Constr. Build. Mater.* **2023**, *368*, 130299. [CrossRef]
26. Kawaai, K.; Nishida, T.; Saito, A.; Hayashi, T. Application of Bio-Based Materials to Crack and Patch Repair Methods in Concrete. *Constr. Build. Mater.* **2022**, *340*, 127718. [CrossRef]

27. Oyewole, O.A.; Maddela, N.R.; Ibrahim, O.H.; Adebayo-Anwo, I.; Adejumo, T.E.; Agbese, E.O.; Egwim, E.C.; Prasad, R. Leveraging the Concretes Calcification with Carbonic Anhydrase Produced by *Alcaligenes faecalis* GA(B) (Mn847724.1). *Bioresour. Technol. Rep.* **2023**, *22*, 101434. [CrossRef]
28. Rosewitz, J.A.; Wang, S.; Scarlata, S.F.; Rahbar, N. An Enzymatic Self-Healing Cementitious Material. *Appl. Mater. Today* **2021**, *23*, 101035. [CrossRef]
29. Mwandira, W.; Mavroulidou, M.; Gunn, M.J.; Purchase, D.; Garelick, H.; Garelick, J. Concurrent Carbon Capture and Biocementation through the Carbonic Anhydrase (CA) Activity of Microorganisms -a Review and Outlook. *Environ. Process.* **2023**, *10*, 56. [CrossRef]
30. Zhang, J.; Yin, Y.; Shi, L.; Bian, H.; Shi, W. Experimental Investigation on Mechanical Behavior of Sands Treated by Enzyme-Induced Calcium Carbonate Precipitation with Assistance of Sisal-Fiber Nucleation. *Front. Earth Sci.* **2022**, *10*. [CrossRef]
31. *BS EN 197-1:2011*; Composition, Specifications and Conformity Criteria for Common Cements. British Standards: London, UK, 2011.
32. *BS EN 812*; Testing Aggregates-Part 112: Methods for Determination of Aggregate Impact Value (AIV). British Standards: Kowloon, Hong Kong, 1990.
33. *ASTM C33-03*; Standard Spesification for Concrete Aggregate. American Society for Testing and Materials: Philadelphia, PA, USA, 2003.
34. Travis Perkins | Builders' Merchant | Building Supplies. Available online: https://www.travisperkins.co.uk/ (accessed on 20 June 2024).
35. ACI Committee 544. *Guide to Design with Fiber-Reinforced Concrete*; American Concrete Institute: Farmington Hills, MI, USA, 2018.
36. *BS EN 12350-2:2019-TC*; Testing Fresh Concrete. Slump-Test. British Standards Institution: London, UK, 2019.
37. *BS 1881: Part 116:1983*; Testing Concrete. Method for Determination of Compressive Strength of Concrete Cubes. British Standards Institution: London, UK, 1983.
38. *ASTM C496/C496M-17*; Standard Test Method for Splitting Tensile Strength of Cylindrical Concrete Specimens. ASTM International: West Conshohocken, PA, USA, 2017.
39. Irshidat, M.R.; Al-Nuaimi, N.; Rabie, M. Thermal Behavior and Post-Heating Fracture Characteristics of Polypropylene Microfiber-Reinforced Geopolymer Binders. *Constr. Build. Mater.* **2022**, *332*, 127310. [CrossRef]
40. Irshidat, M.R.; Al-Nuaimi, N.; Rabie, M. Hybrid Effect of Carbon Nanotubes and Polypropylene Microfibers on Fire Resistance, Thermal Characteristics and Microstructure of Cementitious Composites. *Constr. Build. Mater.* **2021**, *266*, 121154. [CrossRef]
41. Shu, Y.; Song, Y.; Fang, H.; Wang, D.; Lu, W.; Huang, Y.; Zhao, C.; Chen, L.; Song, X. Fiber-Reinforced Microbially Induced Carbonate Precipitation (MICP) for Enhancing Soil Stability: Mechanisms, Effects, and Future Prospects. *J. Build. Eng.* **2024**, *94*, 109955. [CrossRef]
42. Kim, T.-K.; Park, J.-S. Performance Evaluation of Concrete Structures Using Crack Repair Methods. *Sustainability* **2021**, *13*, 3217. [CrossRef]
43. ELE International—Crack Detection Microscope Magnification X 40 Measuring Range of 4 mm in 0.02 mm Divisions. Available online: https://www.ele.com/product/crack-detection-microscope-magnification-x-40-measuring-range-of-4mm-in-0-02mm-divisions (accessed on 11 August 2025).
44. Sbahieh, S.; Rabie, M.; Ebead, U.; Al-Ghamdi, S.G. The Mechanical and Environmental Performance of Fiber-Reinforced Polymers in Concrete Structures: Opportunities, Challenges and Future Directions. *Buildings* **2022**, *12*, 1417. [CrossRef]
45. Rabie, M.; Irshidat, M.R.; Al-Nuaimi, N. Ambient and Heat-Cured Geopolymer Composites: Mix Design Optimization and Life Cycle Assessment. *Sustainability* **2022**, *14*, 4942. [CrossRef]
46. Irshidat, M.R.; Al-Nuaimi, N.; Rabie, M. Sustainable Utilization of Waste Carbon Black in Alkali-Activated Mortar Production. *Case Stud. Constr. Mater.* **2021**, *15*, e00743. [CrossRef]
47. Irshidat, M.R.; Al-Nuaimi, N.; Ahmed, W.; Rabie, M. Feasibility of Recycling Waste Carbon Black in Cement Mortar Production: Environmental Life Cycle Assessment and Performance Evaluation. *Constr. Build. Mater.* **2021**, *296*, 123740. [CrossRef]
48. Finkbeiner, M.; Inaba, A.; Tan, R.B.H.; Christiansen, K.; Klüppel, H.J. The New International Standards for Life Cycle Assessment: ISO 14040 and ISO 14044. *Int. J. Life Cycle Assess.* **2006**, *11*, 80–85. [CrossRef]
49. Blay-Armah, A.; Mohebbi, G.; Bahadori-Jahromi, A.; Fu, C.; Amoako-Attah, J.; Barthorpe, M. Evaluation of Embodied Carbon Emissions in UK Supermarket Constructions: A Study on Steel, Brick, and Timber Frameworks with Consideration of End-of-Life Processes. *Sustainability* **2023**, *15*, 14978. [CrossRef]
50. Mohebbi, G.; Bahadori-Jahromi, A.; Ferri, M.; Mylona, A. The Role of Embodied Carbon Databases in the Accuracy of Life Cycle Assessment (LCA) Calculations for the Embodied Carbon of Buildings. *Sustainability* **2021**, *13*, 7988. [CrossRef]
51. Rabie, M.; Ibrahim, M.; Ebead, U.; Shaaban, I.G. Optimising Sustainable Alkali-Activated Mortar: Experimental Work and Machine Learning Predictions. In Proceedings of the Institution of Civil Engineers-Structures and Buildings, London, UK, 25 July 2025. [CrossRef]
52. Jones, G.H.C. *Embodied Carbon—The ICE Database*; Circular Ecology and University of Bath: Bath, UK, 2019.

53. Hammond, G.; Jones, C. *Inventory of Carbon & Energy: ICE*; Sustainable Energy Research Team, Department of Mechanical Engineering: Bath, UK, 2008; Volume 5.
54. Gültekin, A.; Beycioğlu, A.; Arslan, M.E.; Serdar, A.H.; Dobiszewska, M.; Ramyar, K. Fresh Properties and Fracture Energy of Basalt and Glass Fiber–Reinforced Self-Compacting Concrete. *J. Mater. Civ. Eng.* **2022**, *34*, 04021406. [CrossRef]
55. Nadondu, B.; Surin, P.; Deeying, J. Multi-Objective Optimization on Mechanical Properties of Glass-Carbon and Durian Skin Fiber Reinforced Poly(Lactic Acid) Hybrid Composites Using the Extreme Mixture Design Response Surface Methodology. *Case Stud. Constr. Mater.* **2022**, *17*, e01675. [CrossRef]
56. Abrishambaf, A.; Pimentel, M.; Nunes, S. Influence of Fibre Orientation on the Tensile Behaviour of Ultra-High Performance Fibre Reinforced Cementitious Composites. *Cem. Concr. Res.* **2017**, *97*, 28–40. [CrossRef]
57. Fu, S.; Lauke, B. Effects of Fiber Length and Fiber Orientation Distributions on the Tensile Strength of Short-Fiber-Reinforced Polymers. *Compos. Sci. Technol.* **1996**, *56*, 1179–1190. [CrossRef]
58. Safiuddin, M.; Abdel-Sayed, G.; Hearn, N. Absorption and Strength Properties of Short Carbon Fiber Reinforced Mortar Composite. *Buildings* **2021**, *11*, 300. [CrossRef]
59. Yang, Y.; Lu, P.; Liu, Z.; Dong, L.; Lin, J.; Yang, T.; Ren, Q.; Wu, C. Effect of Steel Fibre with Different Orientations on Mechanical Properties of 3D-Printed Steel-Fibre Reinforced Concrete: Mesoscale Finite Element Analysis. *Cem. Concr. Compos.* **2024**, *150*, 105545. [CrossRef]
60. Li, H.; Li, L.; Li, L.; Zhou, J.; Mu, R.; Xu, M. Influence of Fiber Orientation on the Microstructures of Interfacial Transition Zones and Pull-out Behavior of Steel Fiber in Cementitious Composites. *Cem. Concr. Compos.* **2022**, *128*, 104459. [CrossRef]
61. Safiuddin, M.; Yakhlaf, M.; Soudki, K.A. Key Mechanical Properties and Microstructure of Carbon Fibre Reinforced Self-Consolidating Concrete. *Constr. Build. Mater.* **2018**, *164*, 477–488. [CrossRef]
62. Ji, Y.; Zou, Y.; Wan, X.; Li, W. Mechanical Investigation on Fiber-Doped Cementitious Materials. *Polymers* **2022**, *14*, 1663. [CrossRef] [PubMed]
63. Yuan, Z.; Jia, Y. Mechanical Properties and Microstructure of Glass Fiber and Polypropylene Fiber Reinforced Concrete: An Experimental Study. *Constr. Build. Mater.* **2021**, *266*, 121048. [CrossRef]
64. Guo, R.; Xian, G.; Li, F.; Li, C.; Hong, B. Hygrothermal Resistance of Pultruded Carbon, Glass and Carbon/Glass Hybrid Fiber Reinforced Epoxy Composites. *Constr. Build. Mater.* **2022**, *315*, 125710. [CrossRef]
65. Li, J.; Hajimohammadi, A.; Yu, Y.; Lee, B.Y.; Kim, T. Mechanism of PVA Fiber Influence in Foam Concrete: From Macroscopic to Microscopic View. *J. Mater. Civ. Eng.* **2023**, *35*, 04023447. [CrossRef]
66. Jiang, F.; Deng, W.; Wang, Q.; Gu, Z.; Wang, J. The Influence of Fiber Dispersion on the Properties of MgO Concrete and Engineering Applications. *Materials* **2025**, *18*, 261. [CrossRef]
67. Shi, X.; Ning, B.; Liu, J.; Wei, Z. Effects of Re-Dispersible Latex Powder-Basalt Fibers on the Properties and Pore Structure of Lightweight Foamed Concrete. *J. Build. Eng.* **2023**, *75*, 106984. [CrossRef]
68. Groetsch, T.; Maghe, M.; Creighton, C.; Varley, R.J. Environmental, Property and Cost Impact Analysis of Carbon Fibre at Increasing Rates of Production. *J. Clean. Prod.* **2023**, *382*, 135292. [CrossRef]
69. Stelzer, P.S.; Cakmak, U.; Eisner, L.; Doppelbauer, L.K.; Kállai, I.; Schweizer, G.; Prammer, H.K.; Major, Z. Experimental Feasibility and Environmental Impacts of Compression Molded Discontinuous Carbon Fiber Composites with Opportunities for Circular Economy. *Compos. Part B Eng.* **2022**, *234*, 109638. [CrossRef]
70. Prenzel, T.M.; Hohmann, A.; Prescher, T.; Angerer, K.; Wehner, D.; Ilg, R.; von Reden, T.; Drechsler, K.; Albrecht, S. Bringing Light into the Dark—Overview of Environmental Impacts of Carbon Fiber Production and Potential Levers for Reduction. *Polymers* **2024**, *16*, 12. [CrossRef] [PubMed]
71. Su, Y.; Qian, C.; Rui, Y.; Feng, J. Exploring the Coupled Mechanism of Fibers and Bacteria on Self-Healing Concrete from Bacterial Extracellular Polymeric Substances (EPS). *Cem. Concr. Compos.* **2021**, *116*, 103896. [CrossRef]
72. Feng, J.; Su, Y.; Qian, C. Coupled Effect of PP Fiber, PVA Fiber and Bacteria on Self-Healing Efficiency of Early-Age Cracks in Concrete. *Constr. Build. Mater.* **2019**, *228*, 116810. [CrossRef]
73. Rauf, M.; Khaliq, W.; Khushnood, R.A.; Ahmed, I. Comparative Performance of Different Bacteria Immobilized in Natural Fibers for Self-Healing in Concrete. *Constr. Build. Mater.* **2020**, *258*, 119578. [CrossRef]
74. Zhang, L.; Zheng, M.; Zhao, D.; Feng, Y. A Review of Novel Self-Healing Concrete Technologies. *J. Build. Eng.* **2024**, *89*, 109331. [CrossRef]
75. Tumwiine, H.; Chala, T.; Ssenyonjo, H.; Kirigoola, D.; Al-Fakih, A. On the Use of Self-Healing Materials in Concrete Technology: A Comprehensive Review of Materials, Mechanisms, and Field Applications. *Mater. Today Chem.* **2025**, *48*, 103001. [CrossRef]
76. Xu, J.; Tang, Y.; Wang, X.; Wang, Z.; Yao, W. Application of Ureolysis-Based Microbial CaCO3 Precipitation in Self-Healing of Concrete and Inhibition of Reinforcement Corrosion. *Constr. Build. Mater.* **2020**, *265*, 120364. [CrossRef]
77. Liu, C.; Xing, L.; Liu, H.; Huang, W.; Nong, X.; Xu, X. Experimental on Repair Performance and Complete Stress-Strain Curve of Self-Healing Recycled Concrete under Uniaxial Loading. *Constr. Build. Mater.* **2021**, *285*, 122900. [CrossRef]

78. Guo, Y.; Xiang, K.; Wang, H.; Liu, X.; Ye, Q.; Wang, X. Experimental Study on Self-Healing and Mechanical Properties of Sisal Fiber-Loaded Microbial Concrete. *Mater. Res. Express* **2023**, *10*, 045701. [CrossRef]
79. Xiao, X.; Tan, A.C.Y.; Unluer, C.; Yang, E.-H. Development of a Functionally Graded Bacteria Capsule for Self-Healing Concrete. *Cem. Concr. Compos.* **2023**, *136*, 104863. [CrossRef]
80. Feng, J.; Chen, B.; Sun, W.; Wang, Y. Microbial Induced Calcium Carbonate Precipitation Study Using *Bacillus Subtilis* with Application to Self-Healing Concrete Preparation and Characterization. *Constr. Build. Mater.* **2021**, *280*, 122460. [CrossRef]
81. Baradaran, M.; Sadeghpour, M. Effect of Bacteria on the Self-Healing Ability of Concrete Containing Zeolite. *Innov. Infrastruct. Solut.* **2023**, *8*, 256. [CrossRef]
82. Amiri, Y.; Hassaninasab, S.; Chehri, K.; Zahedi, M. Investigating the Effect of Adding Bacillus Bacteria and Nano-Clay on Cement Mortar Properties. *Case Stud. Constr. Mater.* **2022**, *17*, e01167. [CrossRef]
83. Zhan, Q.; Zhou, J.; Wang, S.; Su, Y.; Liu, B.; Yu, X.; Pan, Z.; Qian, C. Crack Self-Healing of Cement-Based Materials by Microorganisms Immobilized in Expanded Vermiculite. *Constr. Build. Mater.* **2021**, *272*, 121610. [CrossRef]